RSC Advances

PAPER

View Article Online
View Journal | View Issue

Cite this: *RSC Adv.*, 2025, **15**, 25823

Remarkably reduced thermal conductivity and enhanced thermoelectric properties of n-type PbTe *via* Sb and Cu co-doping

Thi Thu Ta,[a] Huu Tuan Nguyen,[b] Duong Van Thiet,[c] Thi Huong Nguyen,[d] Anh Tuan Thanh Pham,[e] Bach Thang Phan,[e] Sunglae Cho[f] and Anh Tuan Duong *[a]

Received 2nd May 2025
Accepted 16th July 2025

DOI: 10.1039/d5ra03099d

rsc.li/rsc-advances

In this study, we demonstrate that co-doping Sb and Cu into n-type PbTe significantly enhances its thermoelectric performance by increasing electrical conductivity and reducing thermal conductivity at high temperatures. A series of $Pb_{1-2x}(SbCu)_xTe$ (x = 0–0.006) samples were synthesized using a solid-state reaction method. The results show that the ZT values at 673 K range from 0.93 to 1.3, depending on the doping concentration. The maximum ZT value of 1.3 at 673 K was achieved for the sample with an optimal doping level of x = 0.005, attributed to the synergistic effects of Sb and Cu on carrier concentration optimization and enhanced phonon scattering. These findings provide a cost-effective and scalable approach to improving the thermoelectric efficiency of n-type PbTe, making it a promising candidate for mid-temperature thermoelectric applications.

1. Introduction

Recently, thermoelectric conversion has emerged as a promising solution to the ongoing energy crisis, offering a clean and renewable energy source.[1] Thermoelectric materials have a unique ability to directly convert heat into electricity and *vice versa*.[2] The efficiency of thermoelectric materials is evaluated using the dimensionless figure of merit (ZT) which is defined as $ZT = S^2\sigma T/\kappa$, where S is Seebeck coefficient, σ is electrical conductivity, $\kappa = \kappa_e + \kappa_l$ is thermal conductivity (where κ_e and κ_l represent the electron and lattice thermal conductivity respectively), and T is the temperature.[3–5] To maximize the ZT value, it is essential to achieve a low thermal conductivity and a high power factor (PF = $S^2\sigma$), making these parameters the primary focus when developing high-performance thermoelectric materials.[6,7]

Over the past 50 years, advancements in thermoelectric materials have paved the way for efficient energy conversion technologies. These materials, capable of directly converting heat into electricity, have attracted significant attention as clean and renewable energy solutions.[8,9] Among inorganic thermoelectric materials, chalcogenides, Si–Ge alloys, skutterudites, clathrates, half-Heusler alloys, and telluride-based compounds such as PbTe and Bi_2Te_3 have demonstrated exceptional thermoelectric performance.[10–15] Among them, lead telluride (PbTe) stands out as one of the most efficient thermoelectric materials for intermediate temperature applications due to its favorable rock-salt crystal structure and intrinsically low thermal conductivity.[16] Notably, PbTe-based thermoelectric devices have been successfully employed in various NASA missions since the development of the first radioisotope thermoelectric generator (RTG) in 1959, which utilized both n-type and p-type PbTe materials for energy conversion.[1,17,18]

Extensive research on PbTe-based materials has revealed that doping plays a crucial role in improving their thermoelectric properties by optimizing carrier concentration.[19–23] Doping has proven to be an effective strategy for achieving these goals, with numerous elements successfully incorporated into PbTe to enhance its n-type thermoelectric properties.[24] In 2011, LaLonde *et al.* investigated the thermoelectric properties of $PbTe_{1-x}I_x$, and the results showed that the average ZT value reached 1.4 in the range of 700–850 K.[25] Subsequently, Yang *et al.* fabricated Bi-doped material based on n-type PbTe doped with Bi, achieving a maximum ZT value of 1.35 at 675 K for the $Pb_{0.99}Bi_{0.01}Te$ sample.[26] By doping transition metals, the carrier concentration can be optimized, increasing both the electrical conductivity and ZT.[27] When Sn and Zn are co-doped, conduction band convergence occurs, improving the Seebeck

[a]*Faculty of Materials science and Engineering, Phenikaa University, Yen Nghia, Ha-Dong District, Hanoi, 12116, Vietnam. E-mail: tuan.duonganh@phenikaa-uni.edu.vn*

[b]*Faculty of Electrical and Electronic Engineering, Phenikaa University, Yen Nghia, Ha-Dong District, Hanoi, 12116, Vietnam*

[c]*School of Mechanical and Automotive Engineering, Hanoi University of Industry, Hanoi, 100000, Vietnam*

[d]*Department of Physics, Nha Trang University, Nha Trang 650000, Vietnam*

[e]*Center for Innovative Materials and Architectures (INOMAR), Vietnam National University, Ho Chi Minh city, Vietnam*

[f]*Department of Physics and Energy Harvest-Storage Research Center, University of Ulsan, Ulsan 680-749, Republic of Korea*

coefficient and resulting in a *ZT* of 1.57 at 840 K.[28] Alternatively, combining chromium as a doping element that can provide e at low temperatures with Ag as an element with the potential to optimize carrier concentration, the thermal conductivity of PbTe decreases and the electrical conductivity increases at high temperatures above 500 K. The *ZT* value reaches ~1.5 at 773 K with a conversion efficiency of ~13.25% for the sample $Pb_{0.975}Cr_{0.025}Te$-1.5%Ag_2Te.[29] However, the *ZT* value of n-type PbTe remains limited compared to p-type materials.[30] Therefore, researching and improving the *ZT* value of n-type PbTe is essential for practical applications.[31]

In particular, Sb doping has been shown to enhance carrier concentration, while Cu doping can reduce lattice thermal conductivity through enhanced phonon scattering. Recent works have reported the synergistic effects of Sb and Cu co-doping in optimizing the thermoelectric properties of n-type PbTe, with significant improvements in *ZT* values.[32,33] Sb is one of the promising n-type doping elements in PbTe.[34] Initially, Christopher M. Jaworski *et al.* found that Sb is an amphoteric nature dopant. Depending on the location of the element it replaces, Sb can be either an acceptor or a donor.[35] Later, Taras Parashchuk *et al.* carried out the impact of Sb substitution on PbTe thermoelectric properties by both experimental and theoretical. As a result, the best conversion efficiency η of 11.7%, obtained with a nominal Sb amount of $x = 0.01$.[36] Furthermore, co-doping Sb with another element into PbTe markedly improved the electric conductivity.[37,38] A *ZT* value of 0.94 was obtained at 723 K for PbTe-based materials co-doping Ag and Sb.[39] Interestingly, the highest *ZT* value to date for n-type PbTe is 1.8 at 773 K by co-doping Sb and I, while p-type PbTe material has the highest value of 2.5.[40–42]

Herein, we carried out a detailed study on the microstructural and fracture face of the series $Pb_{1-2x}(SbCu)_xTe$ samples with different content of Sb and Cu ($x = 0$; 0.003; 0.004; 0.005; and 0.006), were synthesized by solid-state reaction method. The effect of introducing Sb and Cu as co-doing elements on the thermoelectric properties of n-type PbTe was investigated in the range temperature of 300–673 K. With the desire that co-doped Sb and Cu will increase electrical conductivity and reduce thermal conductivity, leading to an improved PF value and *ZT* coefficient.

2. Experiment

2.1. Synthesis

All the high-purity Pb (99.99%), Te (99.99%), Sb (99.99%), and Cu (99.99%) powders were used to produce a series of $Pb_{1-2x}(SbCu)_xTe$ ($x = 0$; 0.003; 0.004; 0.005, and 0.006) solid materials using solid-state reaction process. The preliminary components were firstly weighed according to stoichiometry and then calcined at 873 K in 1 hour under Ar atmosphere after homogenous mixing. After that, the mixture powder was added to graphite die and pressed at 573 K for 1 hour at 5 MPa. The pellets were sintered again under the same conditions. Thereafter, the sintered pellets were cut into a correct sizes for further measurents with a slow cutter.

2.2. Characterization

The phase purity and the crystal structure of the specimens were analyzed carrying out X-ray diffraction measurements by using Cu Kα radiation (XRD EQUNOX 5000, Thermo scientific, France). The temperature dependence Seebeck coefficient and the electrical conductivity were assessed by the standard four-probe method. The thermal conductivity (σ) of the pellets was measured according to the following equation: $\kappa = DC_p\rho$, where D is the thermal diffusivity, C_p represents the specific heat and ρ is density. The D value was measured on a Netsch LFA-457 apparatus in the range of 300–673 K. The microstructure of the fractured surfaces was investigated using Field-Emission Scanning Electron Microscopy (FESEM S4800, Hitachi, Japan).

3. Results and discussion

The X-ray diffraction (XRD) patterns of pristine PbTe and Sb/Cu co-doped PbTe bulk samples are shown in Fig. 1. The diffraction peaks for all samples align closely with the standard JCPDS reference pattern for PbTe (JCPDS, no. 65-0137) confirming that the samples retain the rock-salt (NaCl) structure with *Fm*3*m* symmetry, characteristic of PbTe.[43] The sharp peaks in the diffraction patterns indicates that the samples are well

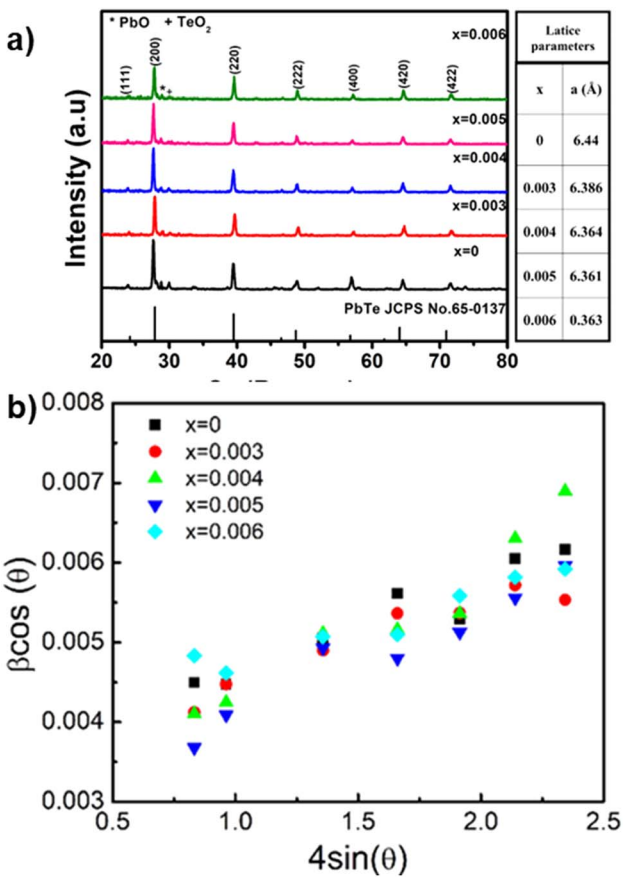

Fig. 1 (a) The room temperature X-ray diffraction and (b) Williamson–Hall (W–H) analysis was performed of $Pb_{1-2x}(SbCu)_xTe$ samples ($x = 0$; 0.003; 0.004; 0.005; and 0.006).

crystallized and exhibit significant grain growth, with a preferred orientation along the (200) plane. The small secondary peaks observed near the (200) peak suggest the presence of TeO_2 (COD-96-153-7587) and PbO (COD-96-153-7983) phases, which likely result from incomplete reactions during the solid-state synthesis.[44] However, no detectable peaks corresponding to Cu_2Te or Sb_2Te_3 phases were observed in the PbTe samples. The lattice parameter for the undoped PbTe sample which was calculated from the XRD data, is approximately 6.44 Å, which is consistent with reported values for bulk PbTe.[37,38] In the Sb and Cu co-doped PbTe, the lattice parameters slightly decrease to 6.386, 6.364, 6.361, and 6.363 Å for $x =$ 0.003, 0.004, 0.005, and 0.006 respectively compared to the undoped sample. The change in lattice parameter can be caused possibly by the Sb and Cu ions which are smaller ions that of Pb in the PbTe lattice. This reduction in lattice parameters validates the incorporation of Sb and Cu into the PbTe lattice and supports the hypothesis that doping introduces dislocations and point defects, contributing to enhanced phonon scattering and reduced thermal conductivity.

To investigate the contributions of strain and crystallite size to the broadening of XRD peaks, a Williamson–Hall (W–H) analysis was performed for the $Pb_{1-2x}(SbCu)_xTe$ samples ($x = 0$, 0.003, 0.004, 0.005, 0.006). The W–H plots of $\beta \cos \theta$ *versus* 4 sin θ exhibited a linear relationship for each composition, allowing the separation of crystallite size and strain effects. The calculated average crystallite sizes ranged from 35.33 to 39.78 nm, with positive microstrain values indicating lattice expansion due to Sb and Cu co-doping. Among the compositions, the sample with $x = 0.005$ exhibited the largest crystallite size (39.78 nm) and the highest strain (0.00034). These results demonstrate that Sb and Cu co-doping induces lattice distortions and point defects, which enhance phonon scattering and contribute to reduced thermal conductivity.

The morphological features of the PbTe and Sb/Cu co-doped PbTe samples are presented in Fig. 2. The absence of visible micro-holes in the SEM images indicates that the bulk materials possess high density. While grain boundaries are not distinctly visible, the morphological contrast shows that the undoped PbTe sample exhibits a different texture compared to the doped samples. At higher magnification, lamellar structures are observed, which are indicative of the brittle fracture mechanism characteristic of these materials. The undoped PbTe sample (Fig. 2b) exhibits long and straight fibrous features across its surface. However, as Sb and Cu are introduced into the PbTe matrix, the number of striped structures increases, as seen in the doped samples (Fig. 2d, f, h and k). This suggests that doping influences the microstructural evolution, potentially impacting the mechanical and thermoelectric properties of the material (Table 1).

Fig. 3a shows the electrical conductivity of all samples as a function of temperature. For undoped PbTe, the electrical conductivity decreases sharply from 81.5 S cm^{-1} at room temperature to 49.6 S cm^{-1} at 500 K before slightly increasing to 52.1 S cm^{-1} at high temperatures. This behavior indicates that PbTe acts as a degenerate semiconductor in the temperature range of 300–500 K.[45] The enhanced electrical conductivity of the doped PbTe samples above 500 K is primarily due to the suppression of bipolar conduction. Particularly, the conductive behavior contributed by both electrons in the conduction band and holes in the valence band becomes more and more significant.[31] Co-doping with Sb and Cu shifts the Fermi level deeper into the conduction band, reducing the contribution of thermally excited minority carriers. Additionally, the increased majority carrier concentration contributes to improved conductivity across the entire temperature range, though its effect is more pronounced at lower temperatures where bipolar conduction is negligible. Therefore, the suppression of bipolar conduction is identified as the dominant mechanism driving the observed increase in electrical conductivity at elevated temperatures. Near room temperature, pristine PbTe shows higher conductivity compared to the doped samples. Fig. 3b presents the net carrier concentration data obtained from Hall effect measurements. The negative values indicate that electrons are the dominant charge carriers. The increasing trend with temperature reflects the combined effects of thermally activated majority carriers and the suppression of minority carrier contribution due to Sb and Cu co-doping. This behavior aligns with the observed suppression of bipolar conduction in the doped samples. The highest conductivity is observed for the $Pb_{0.992}(SbCu)_{0.004}Te$ sample, which exhibits an electrical conductivity of 112.2 S.cm^{-1} at 673 K.

Fig. 4 demonstrates the temperature dependence of the Seebeck coefficient for $Pb_{1-2x}(SbCu)_xTe$ samples with doping concentrations of $x = 0$; 0.003; 0.004; 0.005; and 0.006. All the samples exhibit negative Seebeck coefficient values, confirming that electrons are the dominant charge carriers and the materials are n-type semiconductors. For un-doped PbTe, the Seebeck coefficient increases from 366 μV K^{-1} at room temperature to 432 μV K^{-1} at 523 K. The consistent negative values of the carrier concentration and Seebeck coefficient (Fig. 3b and 4) confirm that electrons remain the dominant carriers above 500 K. The observed decrease in the Seebeck coefficient in co-doped samples is primarily attributed to the increased carrier concentration resulting from Sb and Cu co-doping, which reduces the Seebeck coefficient due to the inverse relationship between S and carrier density. While the suppression of bipolar conduction is achieved by shifting the Fermi level deeper into the conduction band, residual thermal excitation of minority carriers may still contribute to the observed behavior, albeit to a much lesser extent. Additionally, co-doping may influence the electronic band structure, further reducing S at elevated temperatures Among the doped materials, the sample with $x =$ 0.003 exhibits the highest Seebeck coefficient, reaching approximately 451 μV K^{-1} at 523 K, which is comparable to the that of the pristine PbTe compound. As the doping concentration enhances to 0.004; 0.005; and 0.006, the maximum Seebeck coefficients are slightly lower, recorded as approximately 441, 420, and 424 μV K^{-1}, respectively, at 473 K.

Fig. 5 shows the temperature dependence of the power factor for the series samples of $Pb_{1-2x}(SbCu)_xTe$ in the range of 300 K to 673 K. The power factor value strongly depends on conductivity as well as the Seebeck coefficient. While the electrical conductivity shows a significant increase with temperature, the

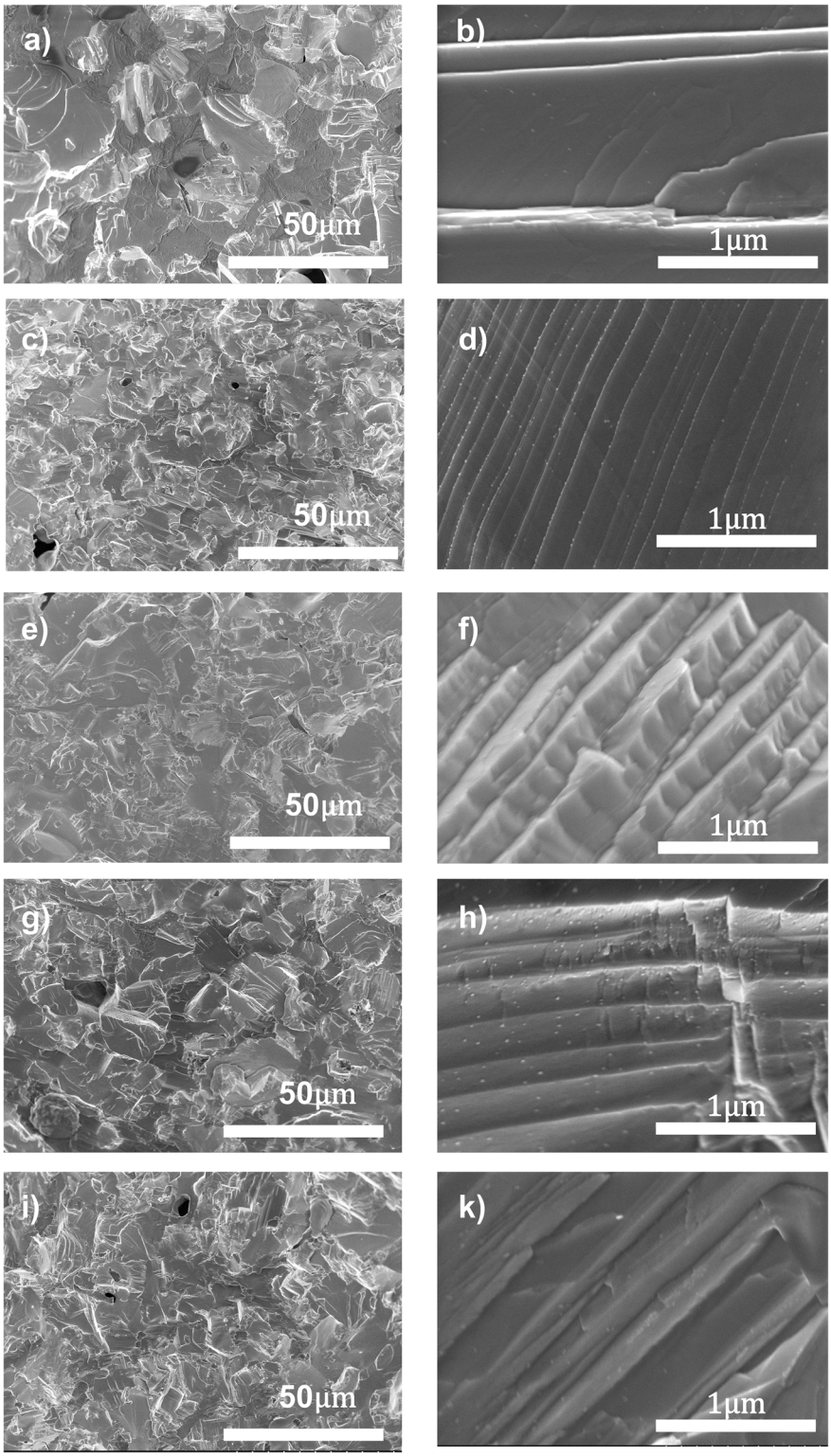

Fig. 2 FE-SEM images show the morphologies of $Pb_{1-2x}(SbCu)_xTe$ samples system: (a and b) $x = 0$, (c and d) $x = 0.003$, (e and f) $x = 0.004$, (g and h) $x = 0.005$, and (i–k) $x = 0.006$ samples.

Seebeck coefficient remains relatively stable. For the undoped PbTe sample, the power factor decreases from 10.9 μW cm^{-1} K^{-2} at room temperature to 8.1 μW cm^{-1} K^{-2} at 673 K. Sb and Cu co-doped samples exhibit an increasing trend power factor in a whole temperature range. In Sb and Cu co-doped samples, the power factor exhibits an increasing trend with temperature. At higher temperatures (above 500 K), this trend is primarily attributed to the enhanced electrical conductivity due to the

Table 1 Crystallite size (D) and strain (ε) of $Pb_{1-2x}(SbCu)_xTe$ (x = 0, 0.003, 0.004, 0.005, 0.006)

Sample (x)	Crystallite size (D) [nm]	Strain (ε)
0	35.33	0.00023
0.003	36.68	0.00024
0.004	37.55	0.00027
0.005	39.78	0.00034
0.006	38.23	0.00028

suppression of bipolar conduction and increased carrier concentration. However, at lower temperatures (below 500 K), the improvement in power factor is mainly driven by the rising Seebeck coefficient, as co-doping does not significantly enhance electrical conductivity in this range compared to the undoped sample. Among the doped samples, the composition with x = 0.005 achieves the highest power factor, reaching approximately 17.2 μW cm^{-1} K^{-2} at 673 K, achieves the highest power factor, reaching approximately. This highlights the beneficial effect of Sb and Cu co-doping on the thermoelectric performance.

Fig. 6 shows the temperature-dependent thermal conductivity of $Pb_{1-2x}(SbCu)_xTe$ samples. For undoped PbTe, the thermal conductivity decreases steadily with increasing temperature up to the onset of the intrinsic region, reaching a minimum value of approximately 1 Wm^{-1} K^{-1} at 573 K. A significant reduction in thermal conductivity is observed with increasing Sb and Cu doping concentrations, which is primarily attributed to the decrease in lattice thermal conductivity. The co-doping of Sb and Cu enhances phonon scattering, effectively reducing lattice thermal conductivity. This effect is likely due to atomic dislocations and point defects introduced by doping, which scatter high-frequency phonons more efficiently. The thermal conductivity of the co-doped samples initially increases with temperature in the 300–400 K range, particularly for the x = 0.004 and x = 0.006 samples. This behavior is attributed to the increased contribution of electron-mediated thermal conductivity due to higher carrier concentration and mobility in the co-doped samples, while phonon–phonon scattering remains weak in this temperature range. As the temperature

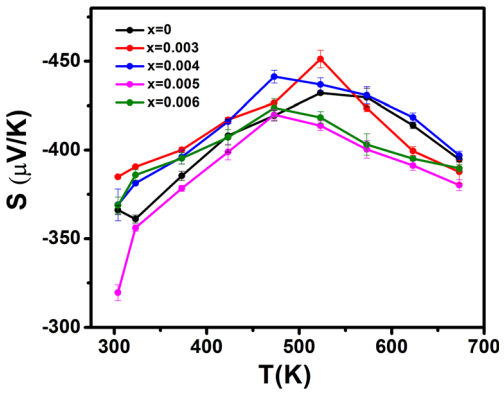

Fig. 4 Temperature dependent Seebeck coefficient of $Pb_{1-2x}(SbCu)_xTe$ samples system.

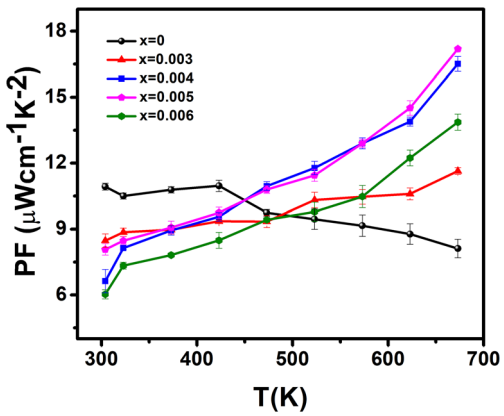

Fig. 5 Temperature dependent power factor of $Pb_{1-2x}(SbCu)_xTe$ samples system.

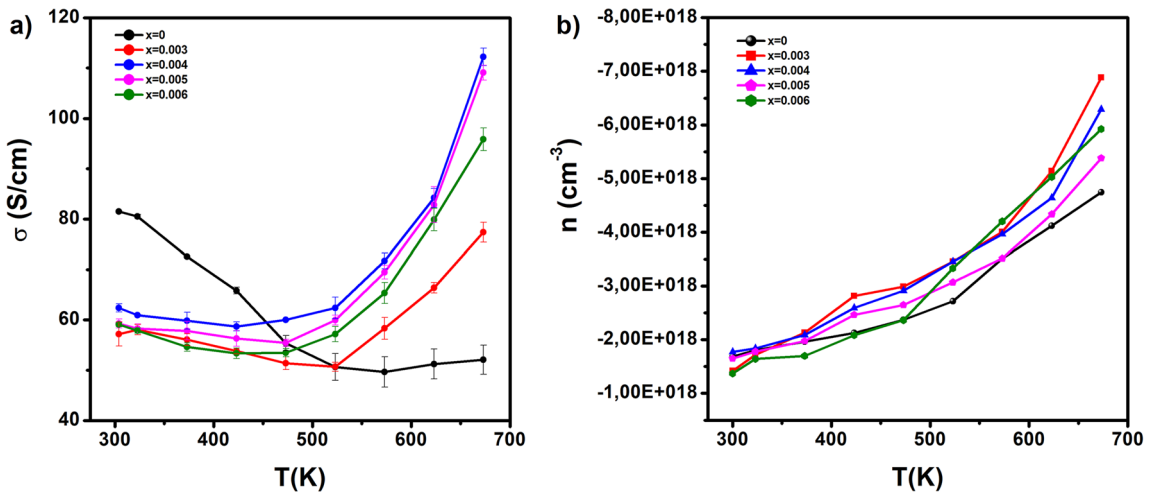

Fig. 3 Temperature-dependent electronic transport properties of $Pb_{1-2x}(SbCu)_xTe$ samples system: (a) electrical conductivity and (b) temperature-dependent net carrier concentration (derived from Hall effect measurements) for $Pb_{1-2x}(SbCu)_xTe$ samples. Negative values confirm that electrons are the majority carriers in the n-type materials.

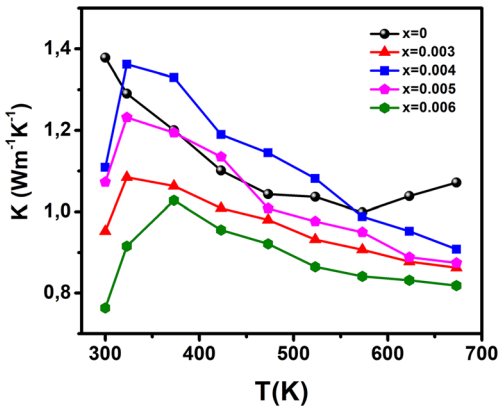

Fig. 6 Temperature dependent thermal conductivity of $Pb_{1-2x}(SbCu)_xTe$ samples system.

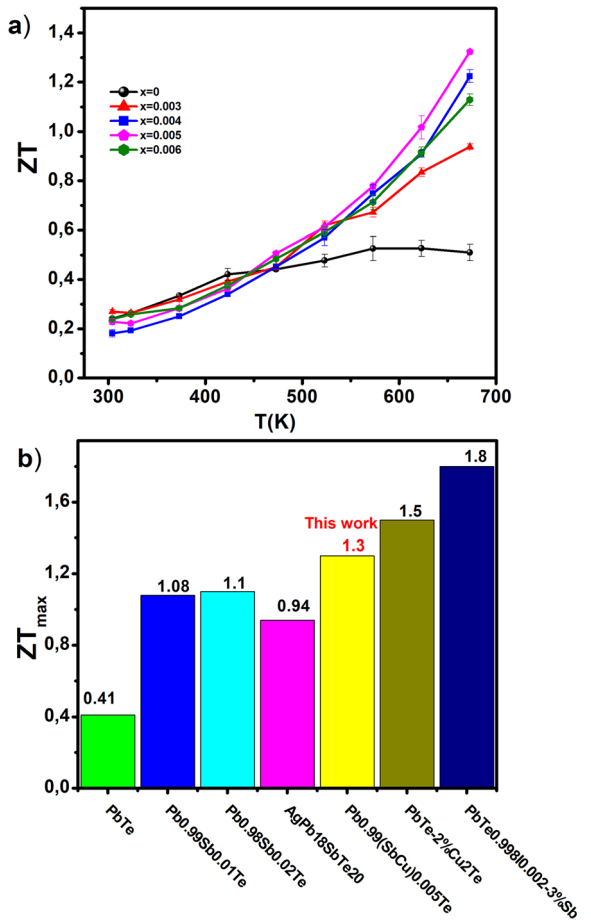

Fig. 7 (a) The thermoelectric figures of merit (ZT) of n-type $Pb_{1-2x}(SbCu)_xTe$ ($x = 0$; 0.003; 0.004; 0.005; and 0.006) samples system; (b) ZT_{max} for represented works and $Pb_{0.99}(SbCu)_{0.005}Te$.

increases further, phonon–phonon scattering becomes dominant, leading to a reduction in lattice thermal conductivity and a subsequent decrease in total thermal conductivity. The $x = 0.004$ sample demonstrates the highest thermal conductivity across most of the temperature range, primarily due to its higher carrier concentration. According to the thermal conductivity formula ($\kappa = \kappa_l + \kappa_e$), the electronic thermal conductivity (κ_e) is strongly dependent on carrier concentration. The elevated carrier concentration in the $x = 0.004$ sample leads to an increase in κ_e, thereby raising the total thermal conductivity. Additionally, the high thermal conductivity in the $x = 0.004$ sample may result from reduced phonon scattering efficiency, which could be attributed to variations in dopant distribution or clustering. Furthermore, stronger electron–phonon coupling in this sample may also contribute to the higher thermal conductivity. Together, these factors counteract the expected reduction in lattice thermal conductivity, resulting in the observed behavior.

The temperature dependence of the figure of merit (ZT), which is calculated from the power factor and thermal conductivity for all $Pb_{1-2x}(SbCu)_xTe$ samples is demonstrated in Fig. 7. For the undoped PbTe sample, a high ZT value of ~0.53 is achieved, which is comparable to the maximum ZT values reported for PbTe samples prepared *via* melting and pulsed electric current sintering in.[36] The addition of Sb and Cu significantly reduces the thermal conductivity due to enhanced phonon scattering, particularly at higher temperatures, which is primarily attributed to the reduction in lattice thermal conductivity. As a result, the ZT value of PbTe improves substantially with increasing temperature and doping levels. For the doped samples, the ZT value ranges from 0.95 to 1.3 at 673 K, depending on the Sb and Cu content. The highest ZT value of 1.3 is achieved at a doping level of $x = 0.005$ which is more than double that of the undoped sample.

Fig. 7b highlights the comparison of the maximum ZT values for n-type PbTe materials. Co-doped Sb and Cu samples exhibit significantly higher ZT values compared to samples doped with Sb alone, underscoring the synergistic effect of co-doping.[6,7] Compared to other co-doping strategies, the optimal ZT value of 1.3 obtained in this study is significantly higher than the previously reported ZT of 0.93 at 723 K for PbTe co-doped with Ag and Sb.[46] However, it remains slightly lower than the ZT value of 1.8 at 723 K observed in PbTe co-doped with Sb and I, as well as some Cu-based alloys.[3,8] These results emphasize the potential of Sb and Cu co-doping to enhance thermoelectric performance in PbTe-based materials, while also highlighting opportunities for further optimization.[47]

4. Conclusion

The $Pb_{1-2x}(SbCu)_xTe$ solid solutions were successfully synthesized, and their thermoelectric properties were enhanced through Sb and Cu co-doping. XRD analysis confirmed the rock-salt structure, with lattice distortions caused by doping contributing to reduced lattice thermal conductivity *via* phonon scattering. Co-doping increased electrical conductivity at high temperatures and maintained competitive Seebeck coefficients, resulting in improved power factors. The thermal conductivity was significantly reduced, with the sample at $x = 0.006$ showing a reduction of approximately 50% reduction compared to undoped PbTe. The optimized composition ($x = 0.005$) achieved

a maximum *ZT* value of 1.3 at 673 K, more than double that of undoped PbTe and higher than many previously reported values for similar systems. These results demonstrate that Sb and Cu co-doping is an effective approach to improving the thermoelectric performance of PbTe, offering potential for further optimization.

Data availability

The data that support the findings of this study are available from the corresponding author upon reasonable request.

Author contributions

T. T. Ta, synthesized the $Pb_{1-2x}(SbCu)_xTe$ samples and performed the electrical conductivity and Seebeck coefficient experiments. H. T. Nguyen, D. V. Thiet, T. H. Nguyen edited the manuscript and performed FE-SEM experiments. A. T. T. Pham, B. T. Phan performed thermal conductivity experiments and edited the manuscript. S. L. Cho edited the manuscript. T. T. Thu wrote the paper with discussion and comments from all the authors. A. T. Duong supervised the project.

Conflicts of interest

The authors have no conflicts to disclose.

Acknowledgements

The research is funded by Vietnam National Foundation for Science and Technology Development (NAFOSTED) under Grant number NCUD.01-2023.17.

References

1 D. T. Duy, V. N. Duy, N. T. Tan, V. M. Dien and P. H. Binh, *Int. J. Thermofluids*, 2025, **25**, 100996.
2 J. Wei, L. Yang, Z. Ma, P. Song, M. Zhang, J. Ma, F. Yang and X. Wang, *J. Mater. Sci.*, 2020, **55**, 12642–12704.
3 B. G. Kim, K. H. Seo, C. H. Lim and S. M. Choi, *J. Mater. Res. Technol.*, 2021, **15**, 606–613.
4 C. Papageorgiou, J. Giapintzakis and T. Kyratsi, *J. Electron. Mater.*, 2013, **42**, 1911–1917.
5 D. Guo, C. Li, K. Li, B. Shao, D. Chen, Y. Ma, J. Sun, X. Cao, W. Zeng and R. Yang, *Phys. E*, 2021, **130**, 114685.
6 R. Aridi, J. Faraj, S. Ali, T. Lemenand and M. Khaled, *Electricity*, 2021, **2**, 359–386.
7 D. Beretta, N. Neophytou, J. M. Hodges, M. G. Kanatzidis, D. Narducci, M. Martin- Gonzalez, M. Beekman, B. Balke, G. Cerretti, W. Tremel, A. Zevalkink, A. I. Hofmann, C. Müller, B. Dörling, M. Campoy-Quiles and M. Caironi, *Mater. Sci. Eng., R*, 2019, **138**, 100501.
8 R. Manghwar, J. Selvaraj, N. Abd Rahim, L. Kumar and H. Khoharo, *Appl. Therm. Eng.*, 2024, **257**, 124231.
9 S. Irfan, Z. Yan and S. B. Khan, *Mater. Sci. Energy Technol.*, 2024, **7**, 349–373.
10 H. Mamur, M. A. Üstüner, H. Korucu and M. R. A. Bhuiyan, *Cleaner Chem. Eng.*, 2023, **6**, 100101.
11 F. H. Sun, H. Li, J. Tan, L. Zhao, X. Wang, H. Hu, C. Wang and T. Mori, *J. Materiomics*, 2024, **10**, 218–233.
12 O. T. Uto, T. J. Ayua and M. U. Sarki, *Next Res.*, 2025, 100316.
13 C. Piscino, G. Latronico, P. Manfrinetti, N. Parodi, R. Spotorno, C. Fanciulli, K. Lohani, T. Bernard, P. Scardi, P. Mele and C. Artini, *J. Alloys Compd.*, 2024, **1009**, 176966.
14 Y. Cui, S. Duan, X. Wang, Q. Tang, J. Xi, X. Liu, Y. Zhang and X. Chen, *J. Materiomics*, 2024, **10**, 783–791.
15 J. Cai, Z. Zhang, L. Chen, C. Han, A. Yang, C. Zhou, Z. Guo, C. Cui, X. Tan, G. Liu, J. Wu and J. Jiang, *Chem. Eng. J.*, 2025, **511**, 162109.
16 H. T. Liu, Q. Sun, Y. Zhong, C. L. Xia, Y. Chen, Z. G. Chen and R. Ang, *Chem. Eng. J.*, 2022, **428**, 132601.
17 M. Darwiche, J. Faraj, K. Chahine, A. Shaito, S. Awad, M. Mortazavi and M. Khaled, *Results Eng.*, 2024, **24**, 103354.
18 B. Cai, H. Hu, H. L. Zhuang and J. F. Li, *J. Alloys Compd.*, 2019, **806**, 471–486.
19 D. Ginting, C. C. Lin, L. Rathnam, J. Hwang, W. Kim, R. A. rahal Al Orabi and J. S. Rhyee, *Data Brief*, 2017, **13**, 233–241.
20 C. Zhu, J. Zhang, H. Ming, L. Huang, Y. Li, T. Chen, D. Li, B. Zhang, J. Xu and X. Qin, *J. Materiomics*, 2021, **7**, 146–155.
21 J. J. Urban, *Joule*, 2019, **3**, 1180–1181.
22 A. Bali, R. Chetty, A. Sharma, G. Rogl, P. Heinrich, S. Suwas, D. K. Misra, P. Rogl, E. Bauer and R. C. Mallik, *J. Appl. Phys.*, 2016, **120**(1–10), 175101.
23 Q. Zhang, H. Wang, Q. Zhang, W. Liu, B. Yu, H. Wang, D. Wang, G. Ni, G. Chen and Z. Ren, *Nano Lett.*, 2012, **12**, 2324–2330.
24 B. Ma, Y. Li, L. Zhu, F. Zhang, X. Li, Y. Shi, P. Liang, Z. Peng, X. Chao, Z. Yang and D. Wu, *Chem. Eng. J.*, 2024, **488**(1–8), 150647.
25 A. D. LaLonde, Y. Pei and G. J. Snyder, *Energy Environ. Sci.*, 2011, **4**(6), 2090–2096.
26 L. Yang, Z. G. Chen, M. Hong, L. Wang, D. Kong, L. Huang, G. Han, Y. Zou, M. Dargusch and J. Zou, *Nano Energy*, 2017, **31**, 105–112.
27 G. Ding, J. Si, S. Yang, G. Wang and H. Wu, *Scr. Mater.*, 2016, **122**, 1–4.
28 L. You, J. Zhang, S. Pan, Y. Jiang, K. Wang, J. Yang, Y. Pei, Q. Zhu, M. T. Agne, G. J. Snyder, Z. Ren, W. Zhang and J. Luo, *Energy Environ. Sci.*, 2019, **12**, 3089–3098.
29 H. T. Liu, Q. Sun, Y. Zhong, Q. Deng, L. Gan, F. L. Lv, X. L. Shi, Z. G. Chen and R. Ang, *Nano Energy*, 2022, **91**, 1–9.
30 Z. Y. Huang, F. Wang, C. Jung, S. Zhang, F. Zu, C. Zhou and Y. Yu, *Mater. Today Phys.*, 2023, **37**, 101198.
31 P. K. Sharma, T. D. Senguttuvan, V. K. Sharma and S. Chaudhary, *Mater. Today Energy*, 2021, **21**, 100713.
32 S. Liu, Y. Yu, D. Wu, X. Xu, L. Xie, X. Chao, M. Bosman, S. J. Pennycook, Z. Yang and J. He, *Adv. Funct. Mater.*, 2021, **31**, 1–11.
33 W. Wu, C. Zhu, H. Ming, T. Chen, D. Li, X. Qin and J. Zhang, *Nanoscale*, 2022, **14**, 17163–17169.
34 G. Dong and Y. Zhu, *Chem. Eng. J.*, 2012, **193–194**, 227–233.

35 C. M. Jaworski, J. Tobola, E. M. Levin, K. Schmidt-rohr and J. P. Heremans, *Phys. Rev. B*, 2009, **80**, 1–10.
36 T. Parashchuk, I. Horichok, A. Kosonowski, O. Cherniushok, P. Wyzga, G. Cempura, A. Kruk and K. T. Wojciechowski, *J. Alloys Compd.*, 2021, **860**, 158355.
37 L. Kungumadevi and G. H. Chandra, *Chem. Phys. Impact*, 2024, **9**, 100736.
38 Z. Yang, S. Wang, Y. Sun, Y. Xiao and L. D. Zhao, *J. Alloys Compd.*, 2020, **828**, 154377.
39 H. Li, K. F. Cai, H. F. Wang, L. Wang, J. L. Yin and C. W. Zhou, *J. Solid State Chem.*, 2009, **182**, 869–874.
40 S. Irfan, Z. Yan and S. B. Khan, *Mater. Sci. Energy Technol.*, 2024, **7**, 349–373.
41 T. Ang, M. Salem, M. Kamarol, H. Shekhar, M. Alhuyi and N. Prabaharan, *Energy Strategy Rev.*, 2022, **43**, 100939.
42 N. Jia, J. Cao, X. Y. Tan, J. Dong, H. Liu, C. K. I. Tan, J. Xu, Q. Yan, X. J. Loh and A. Suwardi, *Mater. Today Phys.*, 2021, **21**, 100519.
43 T. Fu, X. Yue, H. Wu, C. Fu, T. Zhu, X. Liu, L. Hu, P. Ying, J. He and X. Zhao, *J. Materiomics*, 2016, **2**(2), 141–149.
44 T. T. Ta, T. K. Mac, D. H. Manh, T. T. H. Giang, D. S. Lam, D. C. Linh, H. T. Nguyen, B. T. Phan, T. Dang Thanh and A. T. Duong, *Phys. B*, 2023, **670**, 415345.
45 P. Y. Deng, K. K. Wang, H. Y. Sung, W. W. Wu and H. J. Wu, *Cell Rep. Phys. Sci.*, 2023, **4**, 101413.
46 H. Li, K. F. Cai, H. F. Wang, L. Wang, J. L. Yin and C. W. Zhou, *J. Solid State Chem.*, 2009, **182**, 869–874.
47 L. Fu, M. Yin, D. Wu, W. Li, D. Feng, L. Huang and J. He, *Energy Environ. Sci.*, 2017, **10**, 2030–2040.